Experimental validation of a numerical model for the ground vibration from trains in tunnels

Qiyun Jin; David Thompson; Daniel Lurcock; Martin Toward; Evangelos Ntotsios; Samuel Koroma
Institute of Sound and Vibration Research, University of Southampton, Southampton, UK

Mohammed Hussein
Civil & Architectural Engineering Department, College of Engineering, Qatar University, P.O. Box 2713, Qatar

Summary
Ground vibration and ground-borne noise from trains in tunnels are attracting increasing attention from researchers and engineers. They are important environmental issues related with the operation of underground networks in intensively-populated urban areas. An accurate prediction for this train-induced vibration can be very helpful in the implementation of countermeasures to achieve the control of vibration or noise levels. In this paper, a numerical model is introduced based on the 2.5D Finite Element / Boundary Element methodology. The part of the metro line concerned is built with a cast-iron tunnel lining. The tunnel structure and the track are modelled with finite elements while the ground is modelled using boundary elements. Then the 2.5D track-tunnel-ground model is coupled with a multiple-rigid body vehicle model to determine the response caused by the passage of a train. To validate the prediction results, measurements have been carried out of the vibration of the rail, tunnel invert, tunnel wall and ground surface when the train is passing by and these are compared with the predictions with good agreement.

PACS no. 43.50.Lj, 43.40.At

1. Introduction

Ground vibration caused by trains in tunnels is transmitted into nearby buildings and radiated as ground-borne noise, which may be disturbing for the inhabitants of these buildings. This is an important environmental problem for both existing metros and planned new lines. Empirical, analytical and numerical prediction methods can be considered.

The empirical approach avoids the need for the detailed input data and theoretical models required for the calculation approaches, but the realisation of this method depends on obtaining suitable measurement data appropriate to the situation considered. In [1] a procedure is described that uses measured transfer functions and source terms which are combined to predict the vibration for a new line. Additionally, empirical prediction models can be established using databases of field measurements. For example, in [2] two calculation procedures were proposed based on the analysis of more than 3000 measurements.

Analytical approaches have the advantage of being rapid and computationally efficient. In [3, 4] analytical models were successfully developed which give promising prediction results of the ground vibration induced by a passing train. However, these models are limited to simple circular tunnel structures which cannot be too close to the ground surface.

For more complex situations, a numerical approach is useful either to verify the simpler tools or as a prediction method itself. The finite element (FE) and boundary element (BE) methods are most commonly used. With the development of high-performance computers, complex transmission problems can be solved more effectively and realistically. Coupled FE-BE models in 2D and 3D were proposed and compared in [5]. It was found that the 3D results are closer to the absolute vibration levels, although at a much higher computational cost. As a compromise, the so-called 2.5D FE-BE method can provide 3D results but with significantly reduced model size for situations where the structure is invariant in the third direction. In this approach a 2D FE-BE mesh is used and the

problem is solved for a range of wavenumbers in the third dimension. The full 3D solution can be recovered from an inverse Fourier transform over wavenumber. Applications of this approach can be found in [6, 7].

In [8] an alternative approach was used based on a periodic FE-BE model, where the Floquet transform was employed to form the geometry of the tunnel allowing for the periodicity of the tunnel segments. However this is computationally less efficient.

In this paper, a numerical model and the coupling method used for the prediction of train-induced vibration will be introduced. In this model, the tunnel and ground are modelled using a 2.5D FE-BE method, that is, the cross-section of the tunnel and ground is modelled by finite elements and boundary elements while the third direction is represented in the wavenumber domain. This model is coupled with a train represented by a series of vehicles, each given by a 10 degree-of-freedom (DOF) multi-body model. The unevenness of the rail and wheel is used as the excitation to determine the contact forces between them. Then the train-induced vibration is determined by using these forces in combination with the transfer functions obtained from the tunnel-ground model.

The results of the numerical model are compared with measurements obtained as part of the MOTIV project (http://motivproject.co.uk) at a location in London. These include the vibration of the rail, the tunnel and the ground surface during the passage of trains. At the measurement location the train speed is 48 km/h and the tunnel depth is about 20 m (from the surface to the tunnel crown).

2. Model description

The prediction model used here includes three parts: the train, the tunnel/track system and the ground. The train is modelled by four vehicle units, each represented by a multi-body vehicle model. The track-tunnel-ground model is assembled using the WANDS software [9]. The cross-section is represented as a 2D FE-BE model, while the third dimension is modelled in the wavenumber domain. The track and tunnel are represented using finite elements and the ground is modelled using boundary elements. The unevenness of the rail is used as the excitation of the coupled system. The detailed model and coupling method will be explained in the following sub-sections.

2.1. Train model

The train is modelled as a four-vehicle train consisting of two driving cars at the ends and two trailer cars in the middle. Although shorter than the actual seven-coach train, this is sufficient to give an estimate of the average level during a pass-by. Each vehicle is represented as a 10-DOF multi-body model including the pitching motion of the car-body and bogie.

Table I Parameters of vehicle model

Car body	mass	18156 kg
	pitching moment of inertia	2.0×10^6 kg.m^2
Bogie	mass	2096 kg
	pitching moment of inertia	6000 kg.m^2
Unsprung wheelset mass	Trailer car	1220 kg
	Motor car	2308 kg
Primary suspension	stiffness	1.346 MN/m
	viscous damping	21.4 kNs/m
Secondary suspension	stiffness	5.655 MN/m
	viscous damping	22.5 kNs/m
Contact stiffness (two wheels)		2.926 GN/m

Each vehicle is 16 m in length. The distance between bogie centres is 10.4 m and the bogie wheelbase is 1.9 m. The wheel diameter is 0.787 m. The parameters of a vehicle unit are listed in Table I. The car body mass corresponds to the loading when the seats are fully occupied.

2.2. Tunnel, track and ground model

The tunnel, shown in Figure 1, is a cast-iron structure made up of seven segments in each section. The segments are bolted together at their end flanges. These flanges provide additional stiffeners in both the circumferential and the longitudinal directions. The stiffeners in the longitudinal direction are modelled by beam elements. The ones around the circumference are discretely distributed in the longitudinal direction and cannot be realised in WANDS, but can only be simulated in an average sense by increasing the lining thickness. However, it has been found that increasing the lining thickness does not have a large effect on the ground response.

In WANDS, the cast-iron lining is modelled by 8-noded solid elements. The invert is modelled as shown in Figure 2 in which the gravel fillings and

Table II Material properties of the rail, rail pad and tunnel lining

Rail	Vertical bending stiffness	Lateral bending stiffness	Mass per unit length per rail	Damping loss factor
	4.86×10^6 Nm^2	0.96×10^6 Nm^2	56 kg/m	0.01
Rail pad	Stiffness per unit length	Damping loss factor	Pad distance	-
	2.62×10^8 N/m^2	0.12	0.915 m	-
Cast Iron (Grade 20)	Density	Young's Modulus	Poisson's ratio	Loss factor
	7150 kg/m	100 GPa	0.3	0.01

the sleepers under the rail are included as part of the concrete invert. The two rails are modelled as beam elements, while the rail pads are modelled as orthotropic material to simulate the fact that they are actually discretely distributed along the track.

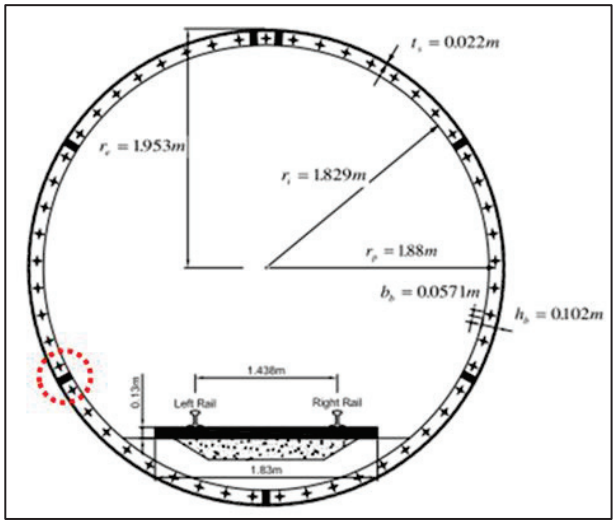

Figure 1 Cross section of the metro tunnel

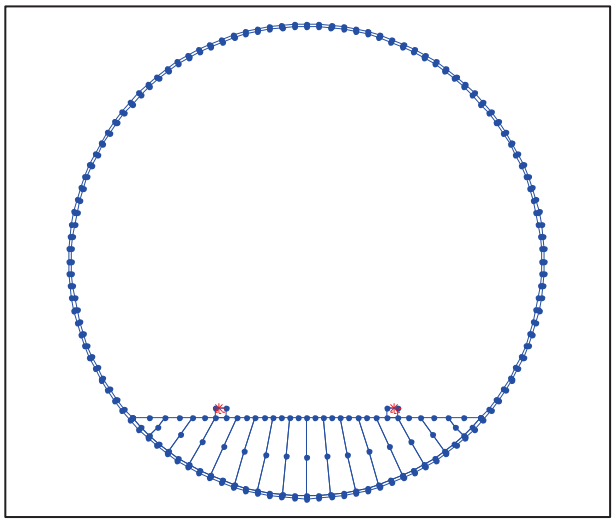

Figure 2 FE model of tunnel and track

All the material properties of track and tunnel are listed in Table II. The properties of the rail pad are averaged over the sleeper spacing. An equal force is applied on each rail.

The soil is formed by boundary elements. The soil properties used in the ground model are based on London clay, with a shear wave speed of 220 m/s and longitudinal wave speed of 1571 m/s [8]. The soil density is 1980 kg/m^3 and loss factor is 0.078.

2.3. Coupling method

The coupling between the train model and tunnel-ground model occurs at the contact between the wheel and rail, as shown in Figure 3. The measured unevenness of the rail, shown in Figure 4, is used as dynamic excitation.

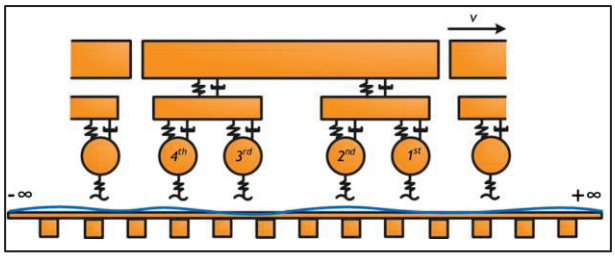

Figure 3 Train model and the coupling with track

As the wheels of the train are running on the same rails, the excitation of all the wheelsets is related by the speed of the train and the distances between them. The equation of motion is given by

$$\left[Y_r + Y_w + Y_c\right]_{4n\times4n}\{F\} = \{T_r\}i\omega r \qquad (1)$$

where F is the force amplitude, r is the unevenness amplitude, and ω is the circular frequency. Y_r, Y_w and Y_c are the mobility of the rail, wheel and contact spring respectively. Y_r and Y_w are obtained from the tunnel-ground model and vehicle model separately while $Y_c=i\omega/k_{\mathrm{Hz}}$ in which k_{Hz} is the stiffness of a Hertzian spring, given in Table I.

A time delay vector T_r is introduced, given by

$$T_r = \{e^{-i\omega x_0(1)/v} \quad e^{-i\omega x_0(2)/v} \quad \cdots \quad e^{-i\omega x_0(n_w)/v}\}^T \qquad (2)$$

where x_0 is the vector of wheelset positions, (1, 2 … n_w indicate the number of wheelsets), and v is the speed of the train.

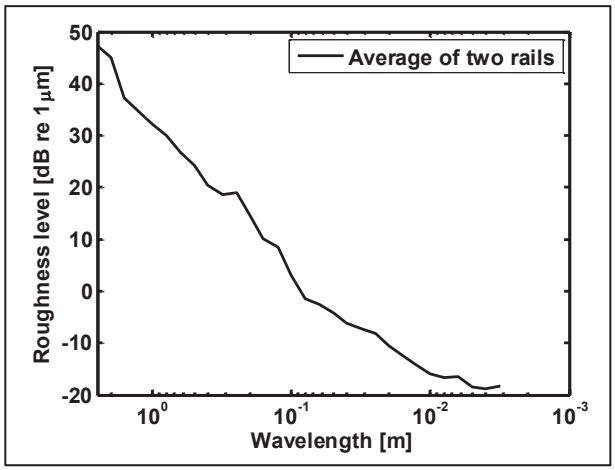

Figure 4 Unevenness spectrum in 1/3 octave bands

3. Result analysis and comparison

3.1. Measurements

A series of measurements was carried out at a location in London. Coordinated measurements took place in the tunnel and on the ground surface. The in-tunnel measurements included: i) the track mobility and decay rate, ii) the rail unevenness as shown in Figure 4, and iii) the train-induced vibration on the rail and tunnel structure (invert and wall). The in-tunnel pass-by accelerations were recorded for both the vertical and lateral directions at two cross-sections. Only the vertical results are shown and these are averaged over the measurements at the two locations. The above-ground measurements consisted of the vibration on the surface of the pavement. Indoor vibration and ground-borne noise measurements were also performed in two buildings (not shown here).

In this paper, the vibration levels to be compared are those measured on the rail, tunnel invert, tunnel wall and ground surface during the passage of train. All the results shown below are expressed as averages over the train length and converted into 1/3 octave band spectra.

3.2. Rail vibration

Figure 5 shows the mobility of the 10DOF vehicle (1st wheel), as well as the mobility of the rail obtained from the tunnel/ground model. The wheel mobility is given for the trailer and motor cars which have different unsprung masses (as shown in Table I). The crossing point between the mobility of the wheel and rail corresponds to the resonance frequency of the coupled vehicle / track system. It can be seen that the mobility of the trailer car is higher than that of the motor car, and consequently the resonance frequency for the trailer car occurs at a slightly higher frequency than for the motor car. All subsequent results are the average of the two types of vehicle.

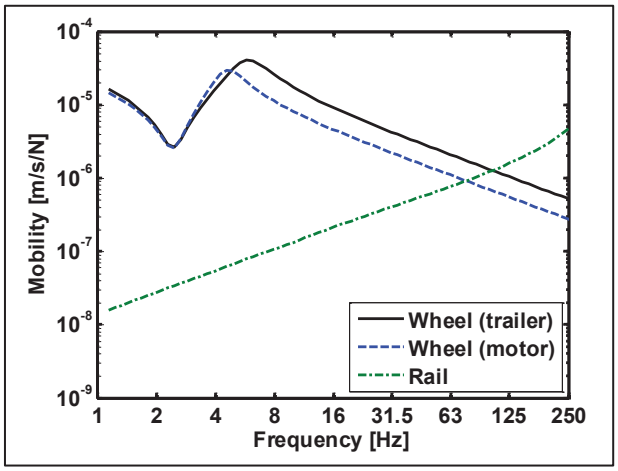

Figure 5 Mobility of wheel and rail

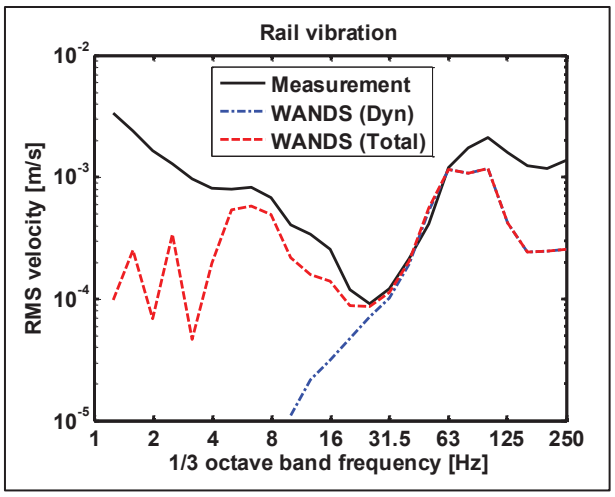

Figure 6 Comparison of rail vibration

Figure 6 compares the rail vibration predicted by the 2.5D FE-BE model with the measurement. The figure shows both the dynamic component of vibration (due to the train-track interaction caused by the wheel/rail unevenness) and the total vibration level, when a train passes at a speed of 48 km/h. The latter includes the quasi-static component of vibration which is also obtained from the WANDS model by setting the excitation frequency of the moving load to zero Hz. Figure 6 shows that, generally speaking, the rail vibration can be well predicted by the 2.5D FE-BE model. The fluctuations at low frequencies (below 8 Hz) are due to the axle spacings, which cannot be

detected in the measurements due to the influence of background noise. At frequencies above 63 Hz, the prediction is about 10 dB lower than the measurements. This is believed to be due to the omission of wheel unevenness.

3.3. Vibration on the tunnel structure

The vertical vibration measured on the tunnel invert and tunnel wall is compared with the prediction results in Figures 7 and 8. The calculation results agree well with the measurements for frequencies between 8 Hz and 63 Hz. The differences at frequencies above 63 Hz are the same as those shown for the rail vibration.

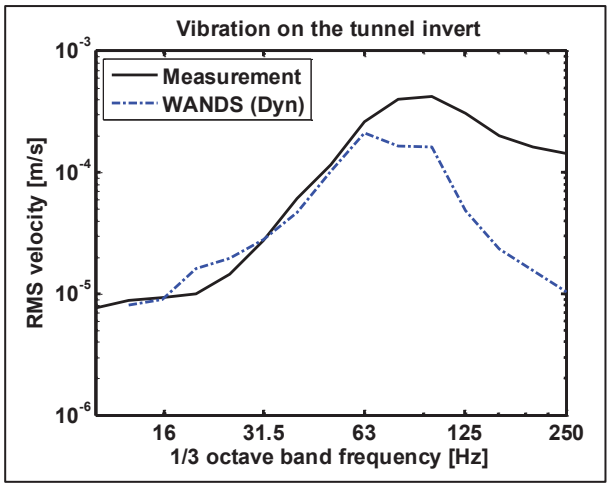

Figure 7 Comparison of vibration on tunnel invert

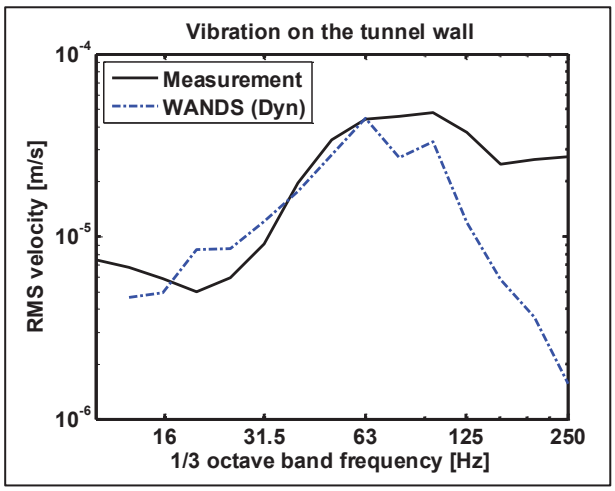

Figure 8 Comparison of vibration on tunnel wall

3.4 Ground vibration

The ground vibration was measured on the pavement above the tunnel. By synchronizing the measurements with those in the tunnel the vibration associated with trains could be extracted. For the far field vibration, the quasi-static component of vibration decays rapidly. Therefore, the ground vibration is dominated by the dynamic component. Figure 9 shows a comparison of the vibration on the ground surface above the tunnel given by the WANDS model and measurements. The background vibration is also shown for comparison. It can be seen that the predictions are generally lower than the measurements. However, the shape of the spectra is quite similar and both have a peak at around 63 Hz.

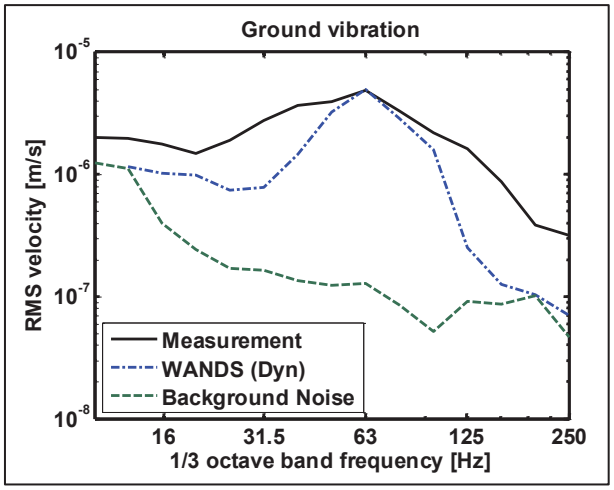

Figure 9 Comparison of ground vibration

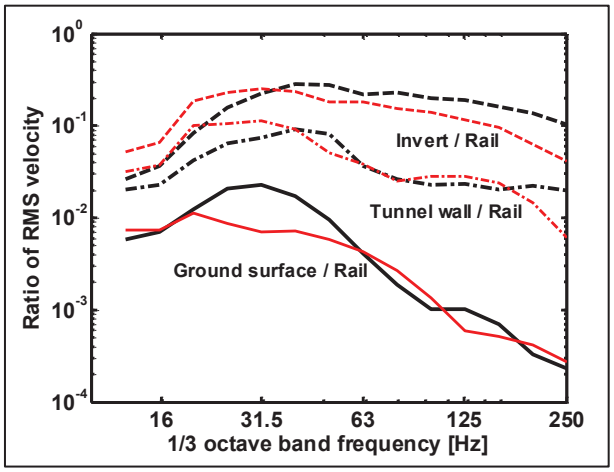

Figure 10 Ratio of the vibration on invert / tunnel wall / ground surface to the vibration on rail
(Thin lines: WANDS; Thick lines: Measurements)

As for the vibration on the rail and the tunnel structure (in Figures 6, 7 and 8), the predicted ground vibration drops quicker than the measurements at high frequency. To demonstrate the consistency of the calculation results, the ratios of vibration on tunnel structure and ground to that on the rail are plotted in Figure 10. It can be seen that the vibration ratios from the prediction results and measurement data agree with each other over the whole frequency range.

This suggests that the differences between measurements and predictions at higher frequencies are due to the unevenness spectrum used which has not included the wheel roughness.

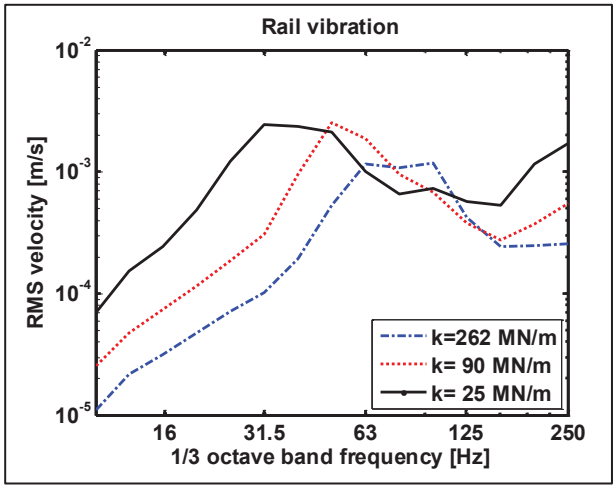

Figure 11 Rail vibration at different rail pad stiffness

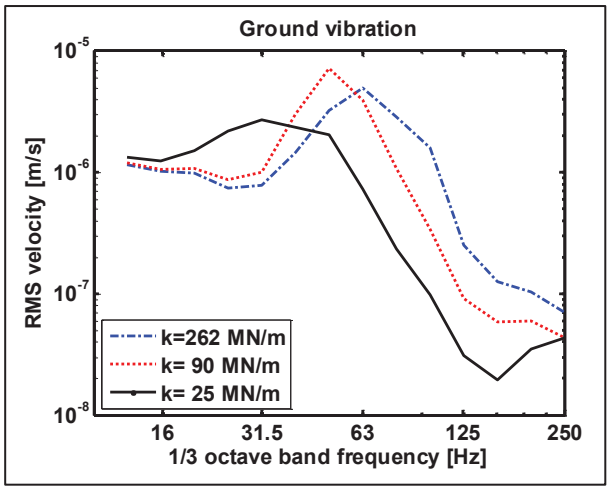

Figure 12 Ground vibration at different rail pad stiffness

3.5 Effect of rail pad stiffness

In Figure 11 and Figure 12, the vibration levels on the rail and the ground surface are shown when three different values are used for the rail pad stiffness. In addition to the conventional rail pad, these values correspond to a soft rail pad and a resilient baseplate. The peaks in the responses, at 31.5, 50 and 63 Hz for rail pads with different stiffness, are the respective resonance frequencies controlled by the mobility of the vehicle and the rail. Below the resonance frequency, the vibration level on the rail increases with the reduction of rail pad stiffness. However, as expected, the soft rail pad gives a reduction in the ground vibration at frequencies above the resonance frequency.

4. Conclusions

A prediction procedure has been proposed for the vibration induced by a train running in a tunnel, based on the 2.5D FE-BE methodology. Both the quasi-static and dynamic components of vibration can be evaluated. Using the coupled train-tunnel-ground model, the vibration levels on the rail and ground surface caused by the train are predicted and compared with the measurements. The results show a good agreement. The effect from varying the rail pad stiffness on the vibration of rail and ground surface is studied, which indicates a practical way of controlling the vibration.

Acknowledgements

The first author is supported by a scholarship from the China Scholarship Council. The experimental work has been supported by the EPSRC research grant EP/K006002/1, “MOTIV: Modelling of Train Induced Vibration”. The authors are grateful to London Underground for their assistance.

References

[1] Transit noise and vibration impact assessment. Office of Planning and Environment, Federal Transit Administration (FTA), FTA-VA-90-1003-06; 2006

[2] R. A. Hood, et al. The calculation and assessment of ground-borne noise and perceptible vibration from trains in tunnels. Journal of Sound and Vibration. 193.1 (1996) 215-225.

[3] J. A. Forrest, H. E. M. Hunt: A three-dimensional tunnel model for calculation of train-induced ground vibration. Journal of Sound and Vibration 294.4 (2006): 678-705.

[4] M. F. M. Hussein, et al. Using the PiP model for fast calculation of vibration from a railway tunnel in a multi-layered half-space. Noise and Vibration Mitigation for Rail transportation systems. Springer, 2008. 136-142.

[5] L. Andersen, C. J. C. Jones. Coupled boundary and finite element analysis of vibration from railway tunnels—a comparison of two-and three-dimensional models. Journal of Sound and Vibration 293.3 (2006) 611-625.

[6] G. Lombaert, G. Degrande. Ground-borne vibration due to static and dynamic axle loads of InterCity and high-speed trains. Journal of Sound and Vibration 319.3 (2009): 1036-1066.

[7] X. Sheng, C. J. C. Jones, D. J. Thompson: Modelling ground vibration from railways using wavenumber finite- and boundary-element methods. Proceedings of the Royal Society A 461.2059 (2005): 2043-2070.

[8] G. Degrande et al., A numerical model for ground-borne vibrations from underground railway traffic based on a periodic finite element-boundary element formulation. Journal of Sound and Vibration 293.3 (2006): 645-666.

[9] C. M. Nilsson and C. J. C. Jones, Theory manual for WANDS 2.1, ISVR Technical Memorandum 975, University of Southampton, (2007).